SAND2011-5109C

3D SIMULATIONS OF THE SELF-MAGNETIC-PINCH DIODE*

Nichelle Bruner,† Dale R. Welch
Voss Scientific, LLC, 418 Washington St SE
Albuquerque, NM, USA

Mark D. Johnston, Bryan V. Oliver
Sandia National Laboratories,‡PO Box 5800
Albuquerque, NM, USA

Abstract

The self-magnetic-pinch diode is being developed as an intense electron beam source for pulsed-power-driven x-ray radiography. In high-power operation, the beam quickly heats the anode, generating a surface plasma. Positive ions drawn from this plasma counterstream with the beam electrons toward the cathode. Although the counterstreaming currents are expected to reach an equilibrium, measurements have shown that the diode impedance steadily falls after peak power is reached. A recent publication described two possible causes of this impedance behavior: anode-plasma expansion into the anode-cathode (A-K) gap and increased ion space-charge near the cathode surface [*Phys. Rev. ST Accel. Beams* 14, 024401 (2011)]. These effects were illustrated using 2D simulations which included the creation and evolution of anode surface plasmas. Here, we report on a follow-on study which determines the impact of 3D effects on plasma expansion. Results show that while azimuthal asymmetries arise, no instabilities are observed.

I. INTRODUCTION

The self-magnetic-pinch (SMP) diode [1, 2, 3, 4] is being developed as an intense electron beam source for pulsed-power-driven x-ray radiography. The diode is composed of a cylindrical cathode with a hollow tip and a planar anode, as illustrated in Fig. 1. The anode is typically a thin foil covering a high-atomic-number material to convert the electron beam into x-rays via bremsstrahlung. The diode is initially in vacuum. As the voltage pulse arrives, high electric field stresses generate space-charge-limited (SCL) electron emission from the cathode. As the electron beam traverses the anode-cathode (A-K) gap, it pinches due to its self-magnetic force, which is balanced by the force of its electric charge.

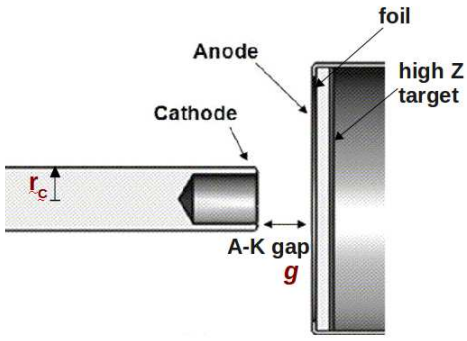

Figure 1. Cross-sectional diagram of the SMP diode. The diode geometries considered here are distinguished by their ratio of A-K gap to cathode radius (g/r_C).

In high-power operation, the beam electrons quickly heat the anode creating a surface plasma of desorbed contaminants and foil material. Positive ions drawn from this plasma counterstream with the beam electrons toward the cathode. The ion space-charge is essential for focusing the electron beam because it partially neutralizes the beam charge, enabling an increased pinch. The counterstreaming currents, referred to as bipolar flow, establish an equilibrium diode impedance that is reduced from the monopolar flow value [5]. However, measurements have shown a third stage in the diode impedance lifetime, occurring

*This work is supported by Sandia National Laboratories and the U.S. Department of Energy under contract number DOA-8910.

†email: Nicki.Bruner@vosssci.com

‡Sandia National Laboratories is a multi-program laboratory managed and operated by Sandia Corporation, a wholly owned subsidiary of Lockheed Martin Corporation, for the U.S. Department of Energy's National Nuclear Security Administration under contract DE-AC04-94AL85000.

after the bipolar flow is reached, which is characterized by a falling diode impedance and a drop in the radiation output [6, 7, 4].

An example of this falling impedance is shown in data from Sandia National Laboratories' Radiographic Integrated Test Stand (RITS-6) pulsed-power accelerator [8]. With a 40-Ω magnetically-insulated transmission line at 10^{-5}-Torr vacuum, the diode nominally produces 150 kA at 7.5 MV. The time-dependent impedances for the diode for different aspect ratios of A-K gap width-to-cathode radius (g/r_C) are shown in Fig. 2. The diode operates as a current-limited device with the equilibrium (or critical) current given by [2, 9]

$$I_{crit} = 8.5\alpha\frac{r_C}{g}(\gamma^2-1)^{1/2} \quad [\text{kA}], \qquad (1)$$

where $\gamma = 1 + eV/m_e c^2$ is the relativistic factor and α is a scale factor used to account for the current increase due to ion space-charge. From Eq. (1) the diode impedance is expected to increase with g/r_C. At relatively early times (< 35 ns), this trend is observed in the measured impedances shown in Fig. 2. At later times, the smallest and largest values g/r_C (1.63 and 2.08) show a rapid fall in impedance, dropping below 10 Ω before the end of the pulse. In contrast, the impedances for the intermediate values of g/r_C fall at a much much slower rate. These dramatic changes in impedance histories occur over a relatively small range of g/r_C values.

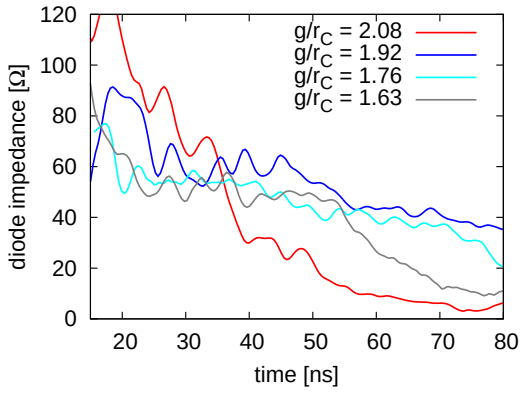

Figure 2. The SMP diode impedance measured on RITS-6 for four values of g/r_C.

A recent publication identifies two mechanisms for this impedance loss: anode plasma expansion into the A-K gap and increased ion space-charge near the cathode surface [10]. These mechanisms were illustrated in 2D simulations which included the creation and evolution of anode surface plasmas. Plasma expansion occurs for all gap widths and has been previously proposed as the impedance-loss mechanism [11, 3]. However, it was demonstrated in Ref. 10 to be the dominant mechanism for the smaller aspect ratios. Larger gaps appear to be more susceptible to increased ion space-charge.

A follow-on study to Ref. 10 is underway to determine the impact of 3D effects on the diode impedance lifetime. The simulation reported here extends the 2D cylindrical (r, z) geometry used in Ref. 10 to 3D cylindrical (r, θ, z). Currently, only $g/r_C = 1.12$ has been modeled. The hybrid particle-in-cell (PIC) technique described in Ref. 12 is again used. This technique is briefly described in Sec. II along with the simulation geometry. 3D results are compared to 2D in Sec. III. Conclusions are summarized in Sec. IV.

II. MODELING THE SMP DIODE

The electrode plasmas created during operation of the SMP diode may be modeled using hybrid algorithms which have been incorporated into the implicit electromagnetic PIC code LSP [13]. These algorithms enable efficient, simultaneous modeling of the dense ($\lesssim 10^{18}$ cm^{-3}) electron and ion populations associated with electrode surface plasmas and the lower-density ($\sim 10^{13} - 10^{15}$ cm^{-3}) populations occurring in bipolar flow [12]. The dense populations are modeled as inertial Eulerian fluids. As the fluid particles accelerate above a prescribed kinetic energy threshold (200 keV is used here), they transition into a kinetic-macroparticle treatment.

Figure 3 shows an $r - z$ cross-sectional view of the geometry used in both the 2D and 3D simulations. The injected voltage pulse has a 7.5-MV peak amplitude and an 8-ns rise. The r, z grid resolution is 80-μm in the A-K gap, with 8 segments in θ.

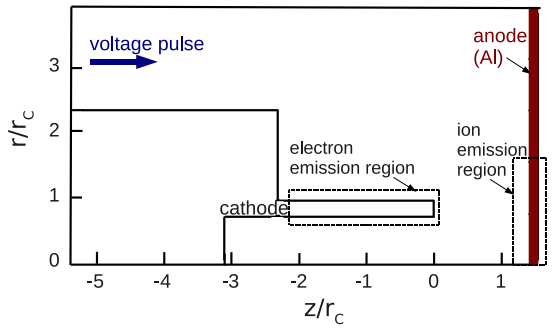

Figure 3. The simulation geometry of the SMP diode. The forward-going voltage wave is injected at the upper left. The region of electron SCL emission is outlined on the cathode. Desorption of the anode plasma occurs in the region outlined on the anode.

SCL electron emission [5, 14] is modeled along the cathode in the region outlined in Fig. 3, with an electric field threshold of 150 kV/cm. The electron beam

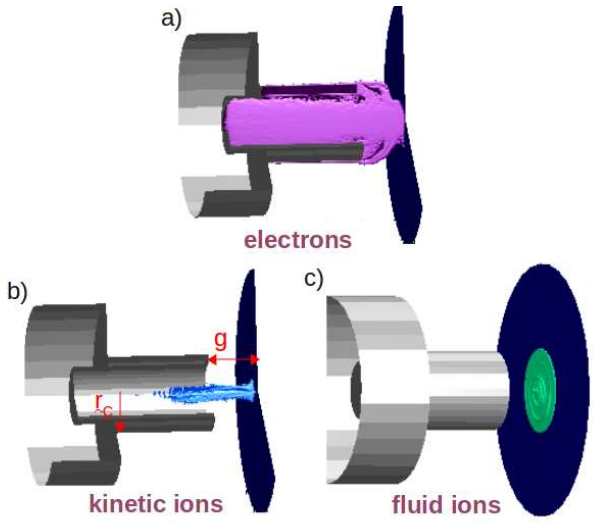

Figure 4. The 3D simulation geometry of the SMP diode with density isosurfaces at 20 ns. a) The electron isosurface at 10^{13} cm^{-3} fills the hollow cathode tip and pinches at the anode shown in blue. b) The kinetic ion isosurface at 3×10^{14} cm^{-3} is located on the z-axis. c) The fluid ion isosurface at 5×10^{14} cm^{-3} lies near the anode surface.

desorbs neutrals from the anode via stimulated desorption (from high-energy electron impact) and thermal desorption (from an increase in surface temperature). The desorption region is also outlined in Fig. 3. The neutrals subsequently fragment to form the plasma, which is composed of carbon or aluminum ions. These species are consistent with spectroscopy results from RITS-6 [15]. Since the anode plasma was dominantly observed expanding into the A-K gap, a cathode plasma is currently not modeled.

The 3D simulation geometry is illustrated in Fig. 4 along with density isosurfaces during the bipolar-flow stage (at 20 ns). The solid objects in Figs. 4a and 4b are cut to show the interior of the cathode tip and the volume occupied by electrons and kinetic ions (C^+), respectively. The highest kinetic ion density occurs on axis. Fluid ions, shown in full 2π in Fig. 4c, reside on the anode surface at 20 ns.

III. MECHANISMS FOR DIODE IMPEDANCE LOSS

In SMP diode simulations without an electrode plasma model, the diode impedance is stable. When we allow for the creation of an anode plasma, all three stages of the impedance lifetime are observed. These are seen in the time-dependent diode impedances plotted in Fig. 5 from 2D and 3D simulations. The 2D results in Fig. 5a cover values of g/r_C from 1.12 to 2.08 and both C^+ and Al^+ plasma species. The first 7 to 9 ns of the pulse is the monopolar stage, after which the impedances drop to the bipolar equilibrium values consistent with Eq. (1). The impedance drop after this stage depends on g/r_C, with the most rapid drops for $g/r_C = 1.12$ and 2.08. The highest impedance stability exists in the mid-range values of g/r_C, consistent with Fig. 2.

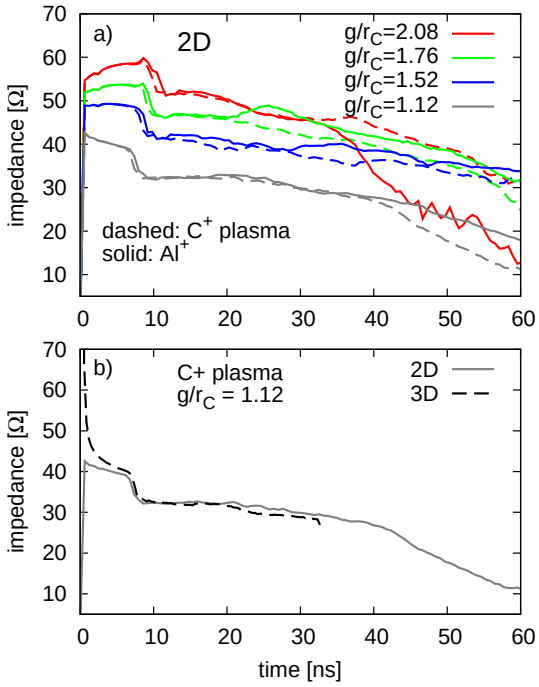

Figure 5. The time-dependent impedance of the SMP diode from a) 2D and b) 3D simulations. Results for four values of the diode aspect ratio are shown in a). The 2D and 3D results for the C^+ anode plasma at $g/r_C = 1.12$ are shown in b).

From Ref. 10, the impedance decline for smaller values of g/r_C is dominated by plasma expansion into the gap, where a higher q/m for the plasma ions leads to faster expansion. The dense plasma advects the anode potential, effectively reducing the gap width and lowering the diode impedance. The impedance stability for larger values of g/r_C is affected by the dynamics of the ions drawn from the anode plasma. Ions with sufficient transverse momenta may exceed r_C before striking the cathode. These ions create greater space charge along the cathode's outer diameter and the electron current increases in response to this space charge.

No 3D effects have been identified in this study which change this description of impedance fall. Figure 6 shows the electron beam density in the x, y plane near the anode surface. While azimuthal asymmetries exist in the beam for the duration of the pulse, similar on scale to the asymmetry in Fig. 6, they are not a

result of instabilities in the diode. The mean x and y positions of the electron and ion beams are plotted as functions of time in Fig. 7. These beam x, y offsets, recorded in the center of the A-K gap, show no evidence of the oscillatory behavior of a hose instability [16, 17], but appear to result from random fluctuations.

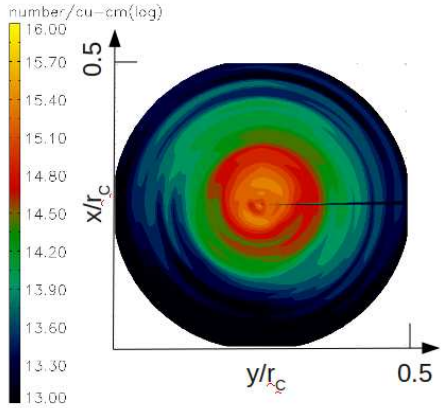

Figure 6. Contour plot of the beam density in the x, y plane (3D) in front of the anode at 28 ns. The plot uses a $\log_{10}$ scale from $10^{13} - 10^{16}$ cm^{-3}.

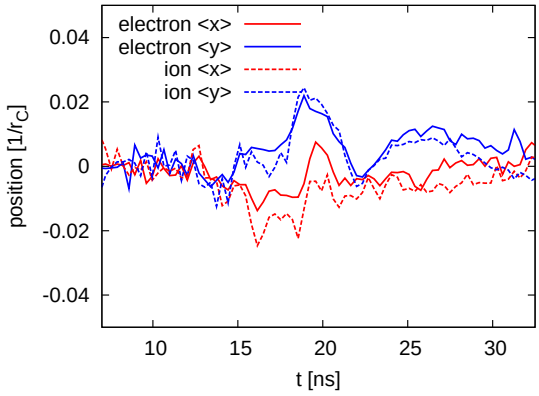

Figure 7. The mean x and y positions of the beam electrons (solid) and kinetic ions (dashed) at the center of the A-K gap from the 3D simulation.

The anode plasma migrates into the the A-K gap, reducing the diode impedance in the same manner as described in Ref. 10. Figure 8 shows $r - z$ contours of the kinetic and fluid ion densities, and the potential integrated from E_z, 32 ns into the (on-going) 3D simulation. The kinetic ions are densest on axis at this time and the plasma, represented by fluid ions, has not migrated a significant distance into the gap. The potential integrated from E_z in Fig. 8 show that the plasma is at the anode potential and an effective gap width may still be determined.

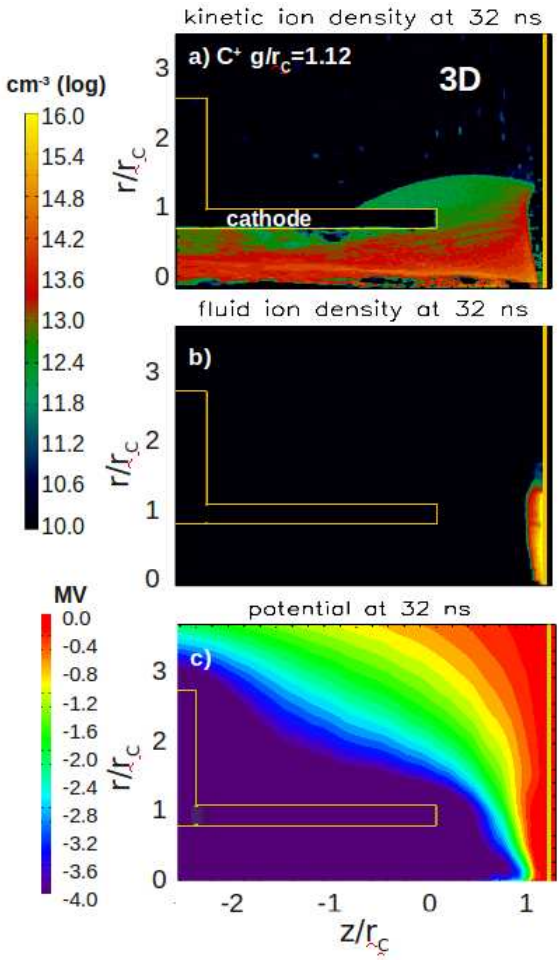

Figure 8. Snapshots of ion density and electric potential in the SMP diode at 32 ns from a 3D simulation. The kinetic ($\geq$ 200 keV) ion density is shown in a). The fluid ion density is shown in b). The density contours are plotted on a $\log_{10}$ scale from $10^{10} - 10^{16}$ cm^{-3}. The gap potential is shown in c) using a linear scale from 0 to -4 MV.

The effective gap is estimated by measuring the distance from the cathode tip to the closest potential maximum. The diode is approximately equal to that calculated using Eq. (1) with the effective gap width in g/r_C. A range of diode-impedance versus effective-gap points were plotted in Ref. 10. That figure is extended to include a 3D point in Fig. 9. The impedances for monopolar and bipolar flow, before plasma expansion, are also shown. The bipolar values, for both the original and effective gaps, are seen to lie close to the impedance function calculated from Eq. (1) with $\alpha = 2.2$ and $V = 7.5$ MV.

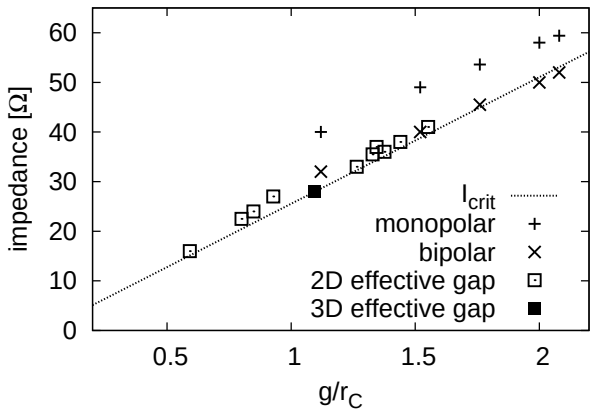

Figure 9. The SMP diode impedance as a function of g/r_C. The "I_{crit}" impedance is calculated from Eq. (1) for $\alpha = 2.2$ and $V = 7.5$ MV. The "monopolar" (electron current only) and "bipolar" (counter-streaming electrons and ions) impedances are determined from 2D simulations. "Effective gap" measurements are made after the anode plasma has extended into the A-K gap and changed the location of the potential maximum.

IV. CONCLUSIONS

Experiments have shown that the SMP diode impedance decreases during the driving voltage pulse, with the most dramatic changes occurring at high and low values of g/r_C. Two mechanisms for this impedance loss are described in Ref. 10: anode plasma expansion into the A-K gap and increased ion space-charge near the cathode surface. These mechanisms were illustrated in 2D simulations which included the creation and evolution of anode surface plasmas using a hybrid, implicit PIC technique.

A follow-on study is being conducted to determine the impact of 3D effects on these mechanisms, with preliminary results reported here. This study extends the 2D cylindrical (r, z) simulation geometry used in Ref. 10 to 3D cylindrical (r, θ, z). A carbon anode plasma was modeled using an aspect ratio of 1.12. The impedance lifetimes are very similar in 2D and 3D for this aspect ratio. Plasma expansion into the A-K gap remains the dominant mechanism for reducing impedance in small-gap diodes, and the impedance is well described by Eq. (1) with an the effective gap. While azimuthal asymmetries arise in the particle densities in the 3D simulation, no instabilities are observed. Late-time behavior will be presented as it becomes available.

Future model improvements will include the effect of cathode plasma evolution. More detailed measurements of the ion species present, their ionization states, relative mixtures, and spatial extents would aid in confirming whether the two mechanisms presented here are responsible for the measured time-dependent impedances.

REFERENCES

[1] J. Threadgold, I. Crotch, D. Rose, and J. Maenchen, "2-D LSP simulations of the self magnetic pinch diode", In *Proc. of the* 14th *IEEE International Pulsed Power Conference*, page 995. IEEE, 2003.

[2] S. Swanekamp, G. Cooperstein, J. Schumer, D. Mosher, F. Young, P.F.Ottinger, and R. Commisso, "Evaluation of self-magnetically pinched diodes up to 10 MV as high-resolution flash X-ray sources", *IEEE Trans. Plasma Sci.*, 32:2004, 2004.

[3] D. Hinshelwood, G. Cooperstein, D. Mosher, D. Ponce, S. Strasburg, S. Swanekamp, S. Stephanakis, B. Weber, F. Young, A. Critchley, I. Crotch, and J. Threadgold, "Characterization of a self-magnetic-pinched diode", *IEEE Trans. Plasma Sci.*, 33:696, 2005.

[4] K. D. Hahn, N. Bruner, S. Cordova, R. Gignac, M. D. Johnston, J. Lechbee, I. Molina, B. V. Oliver, S. Portillo, J. Threadgold, T. J. Webb, D. R. Welch, and D. Ziska, "Overview of Self-Magnetically Pinched-Diode Investigations on RITS-6", *IEEE Trans. Plasma Sci.*, 38:2652, 2010.

[5] C. Litwin and R. Rosner, "Relativistic space-charge-limited bipolar flow", *Phys. Rev. E*, 58(1):1163–1164, Jul 1998.

[6] D. Hinshelwood, R. Allen, R. Commisso, G. Cooperstein, B. Huhman, D. Mosher, D. Murphy, P.F.Ottinger, J. Schumer, S. Swanekamp, S. Stephanakis, B. Weber, F. Young, I. Crotch, J. O'Malley, and J. Threadgold, "High-Power Self-Pinch Diode Experiments for Radiographic Applications", *IEEE Trans. Plasma Sci.*, 35:565, 2007.

[7] S. Portillo, B. V. Oliver, S. Cordova, N. Bruner, D. Ziska, and D. Rovang, "Demonstration of the Self-Magnetic-Pinch Diode as an x-ray Source for Flash Core-Punch Radiography", Technical Report SAND2007-6324, Sandia National Laboratories, October 2007.

[8] D. Johnson, V. Bailey, R. Altes, P. Corcoran, I. Smith, S. Cordova, K. Hahn, J. Maenchen, I. Molina, S. Portillo, E. Puetz, M. Sceiford, D. V. de Valde, D. Rose, B. Oliver, D. Welch, and D. Droemer, "Status of the 10 MV, 120 kA RITS-6 Inductive Voltage Adder", In *Proc. of the* 15^{th} *IEEE International Pulsed Power Conference*, pages 314–317. IEEE, 2005.

[9] B. V. Oliver, K. D. Hahn, M. D. Johnston, and S. Portillo, "Advances in High Intensity e-beam Diode Development for Flash X-ray radiography", *Acta Phys. Pol. A*, 115:1044, 2009.

[10] N. Bruner, D. R. Welch, K. D. Hahn, and B. V. Oliver, "Anode plasma dynamics in the self-magnetic-pinch diode", *Phys. Rev. ST Accel. Beams*, 14(2):024401, Feb 2011.

[11] J. Maenchen, G. Cooperstein, J. O'Malley, and I. Smith, "Advances in Pulsed Power-Driven Radiography Systems", *Proceedings of the IEEE*, 92:1021–1042, 2004.

[12] D. R. Welch, D. V. Rose, N. Bruner, R. E. Clark, B. V. Oliver, K. D. Hahn, and M. D. Johnston, "Hybrid simulation of electrode plasmas in high-power diodes", *Phys. Plasmas*, 16(12):123102, 2009.

[13] D. R. Welch, D. V. Rose, M. E. Cuneo, R. B. Campbell, and T. A. Mehlhorn, "Integrated simulation of the generation and transport of proton beams from laser-target interaction", *Phys. Plasmas*, 13(6):063105, 2006, LSP is a software product of ATK Mission Research.

[14] I. Langmuir and K. Blodgett, "Current limited by space charge between coaxial cylinders", *Phys. Rev.*, 22:347, 1923.

[15] M. D. Johnston, B. V. Oliver, S. Portillo, J. E. Maenchen, T. A. Mehlhorn, D. R. Welch, D. V. Rose, N. Bruner, D. Droemer, Y. Maron, and A. D. Heathcote, "Spectroscopic Analysis of the Self Magnetic Pinch Diode Used in Flash X-Ray Radiography Research", In *Proc. of the* 34^{th} *IEEE International Conference on Plasma Science*, page 445. IEEE, 2007.

[16] T. C. Genoni and T. P. Hughes, "Ion-hose instability in a long-pulse linear induction accelerator", *Phys. Rev. ST Accel. Beams*, 6(3):030401, Mar 2003.

[17] D. Rose, T. Genoni, and D. Welch, "Ion-hose instability growth and saturation for counter-streaming electron and ion beams in an applied magnetic field", *Phys. Plasmas*, 11:4990–4997, 2004.